PNAS
www.pnas.org

Supplementary Information for

Regulatory γ1 subunits defy symmetry in functional modulation of BK channels

Vivian Gonzalez-Perez, Manu Ben Johny, Xiao-Ming Xia, Christopher J. Lingle

Corresponding author: C.J. Lingle
Email: clingle@morpheus.wustl.edu

This PDF file includes:

Supplementary text
Figs. S1 to S8
References for SI reference citations

www.pnas.org/cgi/doi/10.1073/pnas.1804560115

Supplementary Information Text

Data Analysis and fitting of Gaussian distributions. Digitized data were analyzed using Clampfit (Molecular Devices). For non-inactivating currents, conductance values (G) were obtained from the tail currents, while for inactivating currents the peak current was used. G-V data sets were fitted with a single Boltzmann function:

$$G(V) = \frac{G_{\max}}{1 + e^{\frac{zF(V - V_h)}{RT}}}$$

, where V_h represents the voltage of half activation and *z* is the valence of the voltage dependence, with F, R, and T having their usual meaning. Notice that the $\alpha+\gamma1$ injection ratio used (1:4 molar ratio) results in at least 90% of expressed BK channels containing the full $\gamma1$–induced effect(1), in which case the fit to a single Boltzmann distribution provides a good estimation of V_h and *z* for $\alpha+\gamma1$ currents. Macroscopic inactivation time constants (τ_{inact}) were obtained by fitting each current decay to a single exponential function. For estimates of V_h and *z*, all reported values reflect averages and s.e.m. for individual fits to each individual patch, while plots show fitted curve to averaged data.

Single-channel traces were first processed using digital subtraction of leak and capacitive current defined from traces lacking any channel opening. τ_{inact} for each single channel was estimated from the ensemble current of 50-100 identical sweeps recorded at 0 Ca^{2+}. The histogram of τ_{inact} was generated using a bin size of 2 ms and the distribution was fitted to the sum of a 3 or 4 component Gaussian error function of the form:

$$f(x) = \sum_{i}^{n} 0.5 * A_i * \left(ERF\left(\frac{1}{\sqrt{2}} \frac{(x + \frac{bw}{2}) - \tau_i}{\sigma_i}\right) - ERF\left(\frac{1}{\sqrt{2}} \frac{(x - \frac{bw}{2}) - \tau_i}{\sigma_i}\right)\right)$$

where n is the total number of Gaussian components, *bw* is the binwidth, and A_i, τ_i, and σ_i represent the area (number of counts in component), mean τ_{inact}, and standard deviation of each component, respectively, with i=1 for the parameters of the slowest inactivating component, i=2 for the second slower and so on. For each bin, this form returns the expected number of counts for the bin centered on value, x. Each measured τ_i represents the mean of a normally distributed Gaussian population, so the standard deviation of each

mean τ_i estimate should scale such that σ_1 of slowest τ_i component should be larger than for faster components, with $\sigma_{1\geq}\sigma_{2\geq}\ \sigma_{3\geq}\sigma_4$. Each distribution was fit in multiple ways (e.g., **Fig. S6**). First, fitting to the sum of 3 or 4 Gaussian components was done allowing free variation of all fitting parameters (**Fig. S6C,D**). However, standard deviations typically did not follow the expected criteria that $\sigma_{1\geq}\sigma_{2\geq}\ \sigma_{3\geq}\sigma_4$. Such unexpectedly large standard deviations associated with faster components may arise from two factors: first, that the numbers of entries in the histogram may be insufficient to define accurately all aspects of each component and, second, some components may actually arise from multiple components. We therefore also fit the distributions with constraints on the standard deviations such that they obligatorily had to fulfill the criteria that $\sigma_{1\geq}\sigma_{2\geq\ldots}\sigma_n$ (**Fig. 4E-F, Fig. S6A-B**). Finally, we also took advantage of the idea that inactivation results from the independent movement of each inactivation domain to the central cavity of the pore (2). Based on this latter consideration, for some fits, mean values of each component were constrained to scale with the slowest component (**Fig. S6E-F**). Evaluation of the quality of fits therefore takes into account two expectations regarding the behavior of the parameters, first, that components of smaller mean τ_i should have smaller standard deviations and, second, that there should be a relationship between the mean time constants. Fitted curves in **Fig. 4E-F**, and **Fig 5H** were obtained with all τ_i values being independent, but with $\sigma_{1\geq}\sigma_{2\geq\ldots}\sigma_{n.}$ The constraint on standard deviation often forced the standard deviation of all components to be identical. Even without the constraint on the relationship between τ_i values, the fitted mean τ_i values are very close to what is expected for the inactivation rates scaling exactly with the number of free inactivation domains. For the β2γ1Chim distribution, the 4 Gaussian fit yielded a SSQ/n that was 4-fold smaller than for the comparable 3 Gaussian fit (**Fig. 4E-F**). Furthermore, the 3 Gaussian fit to the same distribution required a very large standard deviation, $\sigma_{3,}$ to fit the fastest component, which propagated to the other components (**Fig. 4F**). For a fit with a 3-component Gaussian, if the constraint on standard deviation is relaxed, the best fit is reached with the fastest component having the largest standard deviation of any component, suggestive that this fast component in fact arises from two populations (**Fig. S6**). The superior fit of the 4 component Gaussian along with a better description of how

standard deviation should scale with mean supports the idea that individual channels can contain 1-4 β2γ1Chim subunits (**Fig. 4E-F**). For single channels containing a mix of WT β2 and β2γ1Chim^{IR} subunits, only a 3 Gaussian fit yielded any fit at all (**Fig. 5H**). For the distribution of channels with WT β2+β2γ1Chim^{IR} subunits, a four Gaussian function simply did not fit the distribution. For the three Gaussian fit, the best fit values for τ_1, τ_2, and τ_3 were essentially identical both for the case that the τ_i values were dependent on τ_1 or all τ_i values were independent.

Three-Cube FRET measurements. Tagged constructs were transfected in HEK293 cells, cultured on 35 mm glass-bottom dishes, and used 2-4 days post-transfection. FRET 2-hybrid experiments were performed on an inverted Nikon TE300 Eclipse (40× 1.3 n.a. objective fluorescence microscope with a custom fluorometer system (University of Pennsylvania Biomedical Instrumentation Group) as previous described (3). Excitation light was delivered using a 150W Xenon arc-clamp gated by a computer-controlled shutter. Epifluorescence emission from single cells was isolated using an image-plane pinhole and measured with a photomultiplier tube (PMT). Filter cubes for CFP, YFP, and FRET were as previously described (3). Experiments used a bath Tyrode's solution containing, in mM, 138 NaCl, 4 KCl, 1 $MgCl_2$, 10 HEPES (pH 7.4 adjusted using NaOH), 0.2 $NaHPO_4$, and 5 D-glucose). Autofluorescence and background light scatter were estimated from untransfected cells of similar confluency and subtracted for each filter cube. FRET efficiencies E_A and E_D were computed from CFP, YFP, and FRET cube fluorescence signals from a single cell as previously described (4). The free concentration of donors (D_{free}) and acceptors (A_{free}) were computed assuming an independent and identical binding scheme. The YFP-tagged BK α subunits were assumed to be tetrameric.

In the initial development of the Three-cube FRET method as a tool for ion channel subunit stoichiometry, the method was validated with a variety of soluble CFP-YFP protein pairs clearly establishing that a range of association stoichiometries could be clearly distinguished, even when different donors or acceptors in a complex were not equidistant (3). Furthermore, the method was used to demonstrate the Ca^{2+}-dependence of calmodulin binding to the Cav1.2 channel. Although the conditions of overexpression in the present experiments are similar, there are some differences with the previous

application. In particular, here both donor (CFP-tagged auxiliary subunits) and acceptor (YFP-tagged Slo1) molecules are membrane-associated. As a consequence, both proteins will likely traffic together through intracellular organelles either while moving to the membrane or following retrieval. Thus, some fraction of the FRET signal seems likely to arise from complexes that will not be functional surface channels, although, if donor and acceptor molecules are not assembled, they would simply not contribute to the FRET signal. Furthermore, it might be possible that FRET efficiencies of donor-acceptor complexes in internal membranes may not be identical to those in surface membranes, perhaps dependent on microenvironment and packing. Such issues will require further tests. Irrespective of these issues, a key point is the FRET signals only arise when donors and acceptors are present in the same complex. Typically, the conditions of expression for our FRET and macroscopic current experiments are designed to favor full occupancy of Slo1 α subunits with a given regulatory subunit. A concern in such cases might be that the donor regulatory subunits assemble in aberrant ways with the Slo1 acceptor, such that unexpectedly high numbers of regulatory subunit per channel might be observed. However, irrespective of the locations and condition of complexes contributing to the FRET signals observed here, all donor-acceptor complexes that contribute to the FRET signals exhibit a limiting 1:1 ratio. This provides independent assurance that the limiting stoichiometry observed from the electrophysiological experiences is not compromised by aberrant subunit assemblies. To further validate that partial stoichiometries can be observed, we undertook a set of experiments in which WT β2 was coexpressed with Slo1-YFP α and β2γ1Chim-CFP (Fig. S8). This competition experiment reveals that, as the relative amount of WT β2 message is increased, there is a reduction in the average number of β2γ1Chim-CFP molecules per channel complex.

Statistical analysis, Macroscopic and single channel data were analyzed with Clampfit (Molecular Devices), Excel (Microsoft), or in-house function fitting software utilizing a Levenberg-Marquardt non-linear least squares fitting algorithm. Data are presented as mean $\pm$ s.e.m. and n represents either the number of cells or number of patches. V_h and z values from Boltzmann fits represent mean values and s.e.m. from averaging of values from the fits to each individual patch. Comparisons among V_h from different constructs were done with the non-parametric Kolmogorov-Smirnov (KS) test which makes no

assumptions about normality of a distribution. When a KS test was used, at least 10 individual GV curves from each construct under a given condition were generated. For $\alpha+\gamma1$ and $\alpha+\beta2\gamma1$Chim, V_h values were indistinguishable (KS P=0.675), but each differs from α and $\alpha+\beta2$ (P=0.000). For single channel Po/V curves (Fig. S7), V_h values for fast and slower inactivating channels were grouped and compared to that of $\alpha+\gamma1$ and found indistinguishable ($\gamma1$ GV vs. $\beta2\gamma1$Chim Po/V: T-test, unpaired; P=0.796). For confidence limits on a Gaussian function fit, best fit values report the mean and the 95% confidence limit (c.l.). For FRET measurements, each point on E_A versus D_{free} and E_D versus A_{free} plots corresponds to an individual transfected cell, from multiple transfections. Estimates of mean and s.e.m. for E_A and E_D were obtained from averages of transfected cells in the saturating range of D_{free} and A_{free}, respectively.

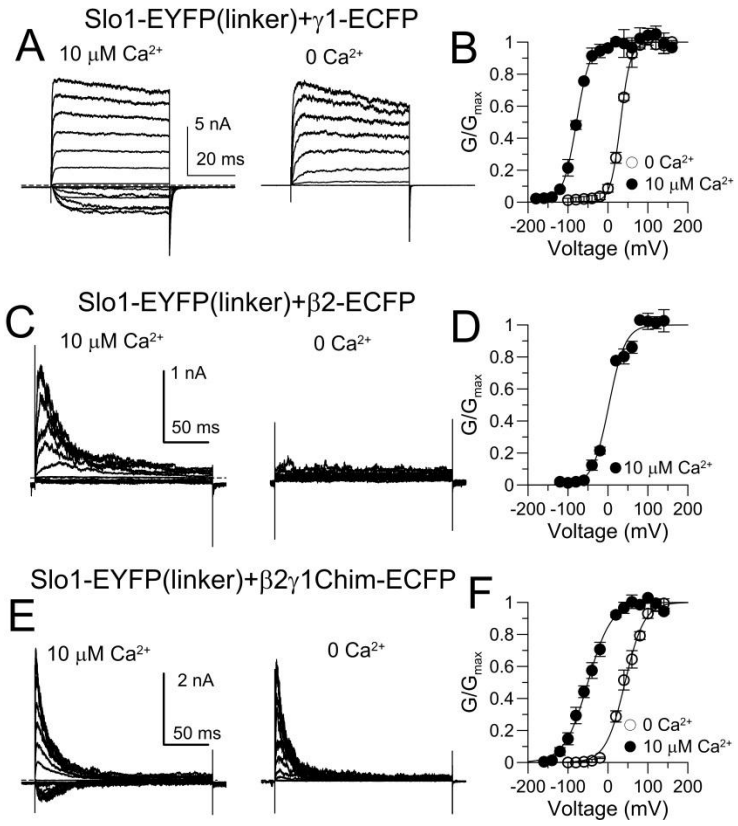

Fig. S1. γ1-ECFP and β2-ECFP function normally when coexpressed with eYFP-tagged Slo1 α subunits in oocytes. (A) ECFP-tagged γ1 subunits were coexpressed with mSlo1 α-EYFP(linker) in *Xenopus* oocytes and currents were activated by voltage steps up to +140 mV in inside-out patches bathed with 10 μM (left) or 0 (right) Ca^{2+}. **(B)** The GV curves (measured from tail currents) at both 0 and 10 μM Ca^{2+} are shifted approximately -120 mV relative to α subunits expressed alone. At 0 Ca^{2+}, V_h=34.5±2.5 mV, *z*=1.58±0.19*e* (n=4) and, at 10 μM Ca^{2+}, V_h = -82.1±4.5 mV, *z*=1.56±0.03*e* (n=4). **(C)** ECFP-tagged β2 subunits were coexpressed with mSlo1-EYFP α subunits and currents recorded at 10 μM (left) and 0 (right) Ca^{2+}. Currents exhibit inactivation behavior typical of WT β2 subunits with minimal activation at 0 Ca^{2+}. **(D)** GV curve for channels with tagged β2 subunits was generated from peak current activated with 10 μM Ca^{2+}, exhibiting an approximately -40 to -50 mV shift (V_h = 2.8±0.9 mV, *z*=1.27±0.15*e* (n=3) compared to Slo1 α alone. **(E)** ECFP-tagged β2γ1Chim subunits were coexpressed with EYFP-tagged Slo1 subunits and currents recorded at 10 μM and 0 Ca^{2+}, as indicated. Note robust activation and inactivation at both [Ca^{2+}]. **(F)** GV curves for the tagged chimera are shown for 0 (V_h=43.0±4.5 mV, *z*=1.1±0.08*e*, n=4) and 10 (V_h = -50.4 ± 5.0 mV, *z*=0.91±0.08*e*, n=4) μM Ca^{2+}. V_h for activation of α+β2γ1Chim currents at 10 μM Ca^{2+} is similar to that for the tagged α+γ1 subunits (**panel A-B**), but currents also show inactivation consistent with the effect of the β2 N-terminus (**panel C**). GVs for the chimeric construct were measured from peak currents.

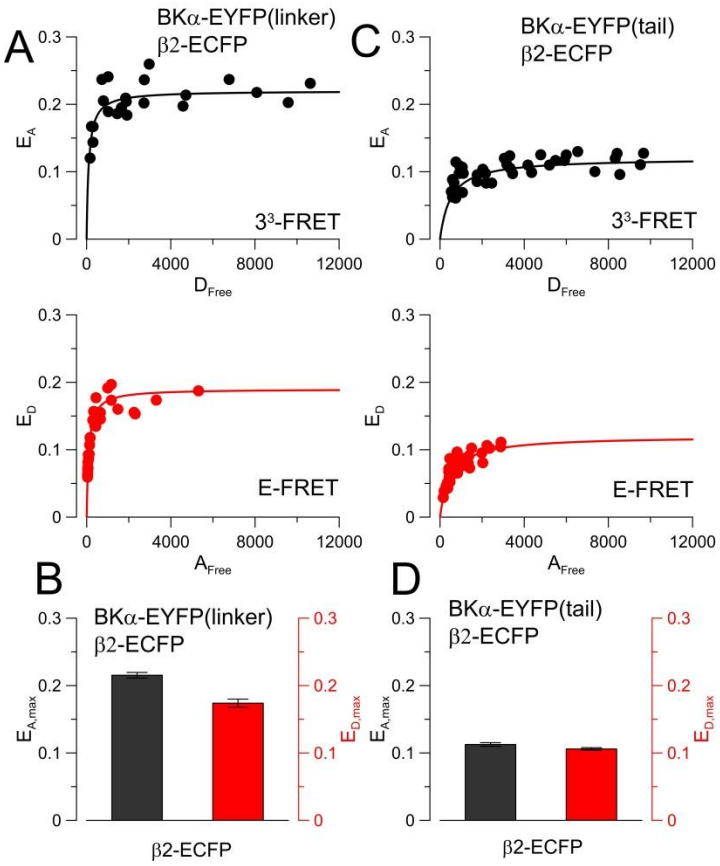

Fig. S2. FRET measurements indicate that up to four β2 subunits can be present in a single β2-containing BK channel. (A) 3^3-FRET efficiency (E_A) is plotted against estimated free donor concentration (D_{free}) with each point representing a single cell, for the α-YFP(linker):β2 combination (Top). (Bottom) E-FRET efficiency (E_D) is plotted as a function of estimated free acceptor concentration (A_{free}). **(B)** Mean (±s.e.m.) values for $E_{A,max}$ (black) and $E_{D,max}$ (red) estimates are shown for the BK α-EYFP linker construct expressed with β2-ECFP. **(C)** Panels show results similar to those in **(A)** but for an EYFP donor on the C-terminus of the BK α subunit. **(D)** Mean (±s.e.m.) values for $E_{A,max}$ (black) and $E_{D,max}$ (red) estimates are shown for the BK α-EYFP tail construct expressed with β2-ECFP.

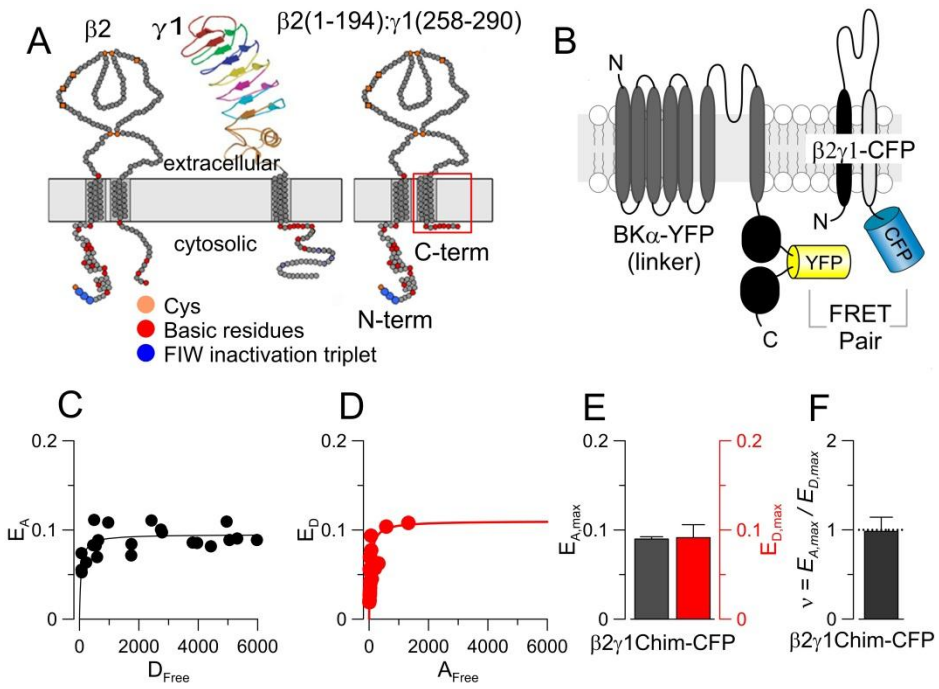

Fig. S3. The β2γ1Chim construct and Slo1 α assemble in an up to 1:1 ratio. (**A**) On the left, likely transmembrane topology of the β2 and γ1 subunits are illustrated. For β2, extracellular cysteines are tan circles, the hydrophobic FIW inactivation triplet is in blue, while, for both β2 and γ1, cytosolic basic residues are red. On the right, the chimeric β2γ1 (β2γ1Chim) construct is shown containing residues 1-194 of β2 and residues 258-290 of γ1. The γ1 TM segment and C-terminus (red box) replaces the β2 TM2 and C-terminus. (**B**) FRET pairs used to define stoichiometry of β2γ1Chim-CFP assembly with BKα-YFP. (**C**) E_A is plotted against estimated free donor concentration (D_{free}) as in previous figures, for the α-YFP(linker):β2γ1Chim-CFP combination (**D**) E-FRET efficiency (E_D) is plotted as a function of estimated free acceptor concentration (A_{free}). (**E**) Mean (±s.e.m.) values for $E_{A,max}$ (black) and $E_{D,max}$ (red) estimates are shown for the BK α-EYFP linker construct expressed with β2γ1Chim-CFP. (**F**) The stoichiometry ratio is plotted for the BKα–YFP(linker):β2γ1Chim-CFP FRET pair confirming an up to 1:1 stoichiometry.

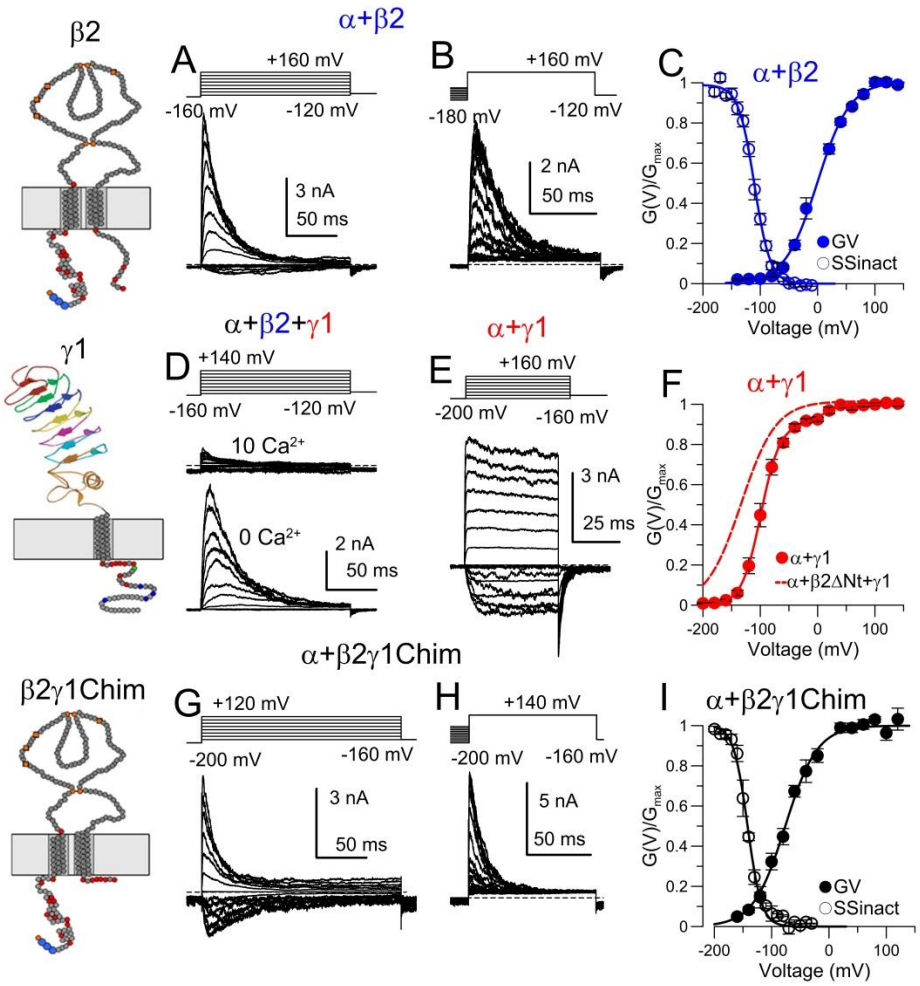

Fig. S4. Comparison of macroscopic activation and steady-state inactivation behavior for α+β2, α+γ1, α+β2+γ1, and the β2γ1Chim construct. Left column shows schematics for various constructs: on the top, β2, in the middle, γ1, and on the bottom, β2γ1Chim. **(A)** Activation of α+β2 currents with 10 μM Ca^{2+}. (**B**) Steady-state inactivation for α+β2 currents with 10 μM Ca^{2+}. **(C)** Activation GV (n=6 patches) and steady-state fractional availability curves (n=7 patches) for α+β2 channels. For activation, V_h=6.7±2.4 mV, *z*=0.96±0.03*e*, while for fractional availability, V_h = -110.8±2.3 mV, with *z*=-1.81±0.11*e*. **(D)** Sets of activation traces for BK α coexpressed with both β2 and γ1 at either 10 μM cytosolic Ca^{2+} (top) or 0 Ca^{2+} (bottom). Because the steady-state fractional availability shifts with the activation curve, at a holding potential of -160 mV, all α+β2+γ1 channels at 10 μM Ca^{2+} are essentially already inactivated at -160 mV. **(E)** Activation traces for α+γ1 with the indicated protocol for 10 μM Ca^{2+}. **(F)** GV curve generated from 8 patches for α+γ1 currents (at 10 μM Ca^{2+}) yields V_h= -95.1±3.9 mV, *z*=1.4±0.05*e*. For comparison, coexpression of γ1 together with an inactivation removed β2 variant shifts the GV (at 10 μM Ca^{2+}) to even more negative potentials (red line), V_h = -134.7±8.8 mV. The gating shift produced by β2γ1Chim is essentially indistinguishable from the effect of γ1 alone, while coexpression of β2+γ1

with Slo1 α results in larger gating shifts suggesting that in the chimera the full β2-mediated effect on gating is not preserved. **(G)** Macroscopic α+β2γ1Chim currents evoked with the indicated protocol in an inside-out patch showing activation at 10 μM cytosolic Ca^{2+}. Voltage step sizes were 20 mV for current activation, and then 10 mV in the steady-state inactivation protocols. **(H)** Currents for α+β2γ1Chim using the indicated protocol to define steady-state inactivation with 10 μM Ca^{2+}. **(I)** Averaged GV (n= 5 patches) for activation for α+β2γ1Chim currents and then fractional availability curves (n= 3 patches) from the steady-state inactivation protocol, for 10 μM Ca^{2+} in both cases. For activation, V_h = -77 ± 3.6 mV, z = 0.90±0.07e. For steady-state inactivation, V_h = -142±1.5 mV with z=-1.95±0.05e.

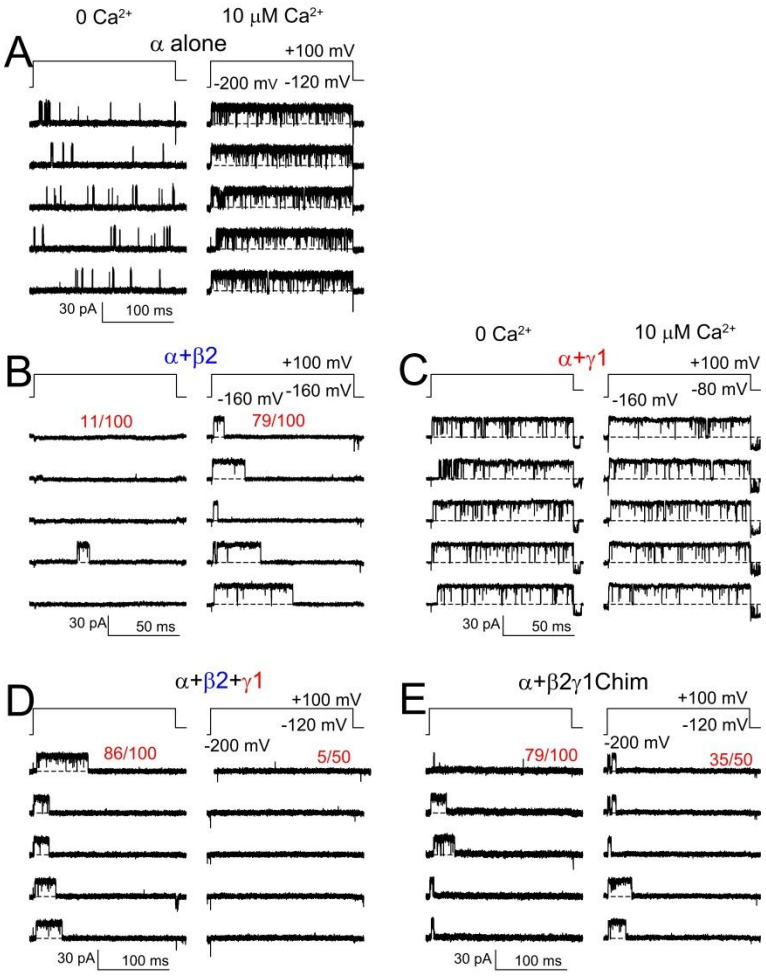

Fig. S5. Examples of single channel traces used to define likelihood of opening for different constructs during a voltage step to +100 mV. We use an empirical measure, the likelihood of observing an opening during a 100 or 200 ms step to +100 mV with 0 Ca^{2+}, to assess ability of a regulatory subunit to shift gating at 0 Ca^{2+}. For a channel which inactivates, null sweeps could arise from channels which are inactivated prior to the voltage step, but a negative prepulse (-160 or -200 mV) is used to minimize this possibility. Thus, for comparisons among channels which inactivate, where direct measures of Po cannot be done directly, the likelihood of opening, provides a reasonable measure of the ability of that channel combination to activate at 0 Ca^{2+}. The likelihood of opening determined for inactivating channels are not directly comparable to subunit combinations lacking an inactivation domain, since in the absence of inactivation they may open at high likelihood, but only to be very low Po. **(A)** Single channels from expression of Slo1 α alone are shown at 0 and 10 μM Ca^{2+}. With α alone, channel opening is likely to occur at +100 mV with high likelihood during 100 ms, but overall open probability (Po) is low, while at 10 μM, channels reliably open to high Po. **(B)** Single channel openings for α+β2 at 0 and 10 μM Ca^{2+}. Numbers show the number of sweeps with openings over the total sweeps. α+β2 channels rarely open at +100 mV with 0 Ca^{2+}, but open with a likelihood of 0.8 or higher with 10 μM Ca^{2+} at +100 mV. **(C)**

α+γ1 channels open to high Po at both 0 and 10 μM Ca^{2+} at +100 mV. **(D)** α+β2+γ1 channels open with high likelihood at 0 Ca^{2+}, but at 10 μM Ca^{2+} are largely constitutively inactivated even from prepulses of -200 mV. **(E)** α+β2γ1Chim openings occur with high likelihood at both 0 and 10 μM Ca^{2+} from a prepulse of -200 mV, since the β2γ1Chim construct does not produce a β2-mediated shift effect. Statistics for the likelihood of opening for sets of patches are shown in **Fig. 4G**.

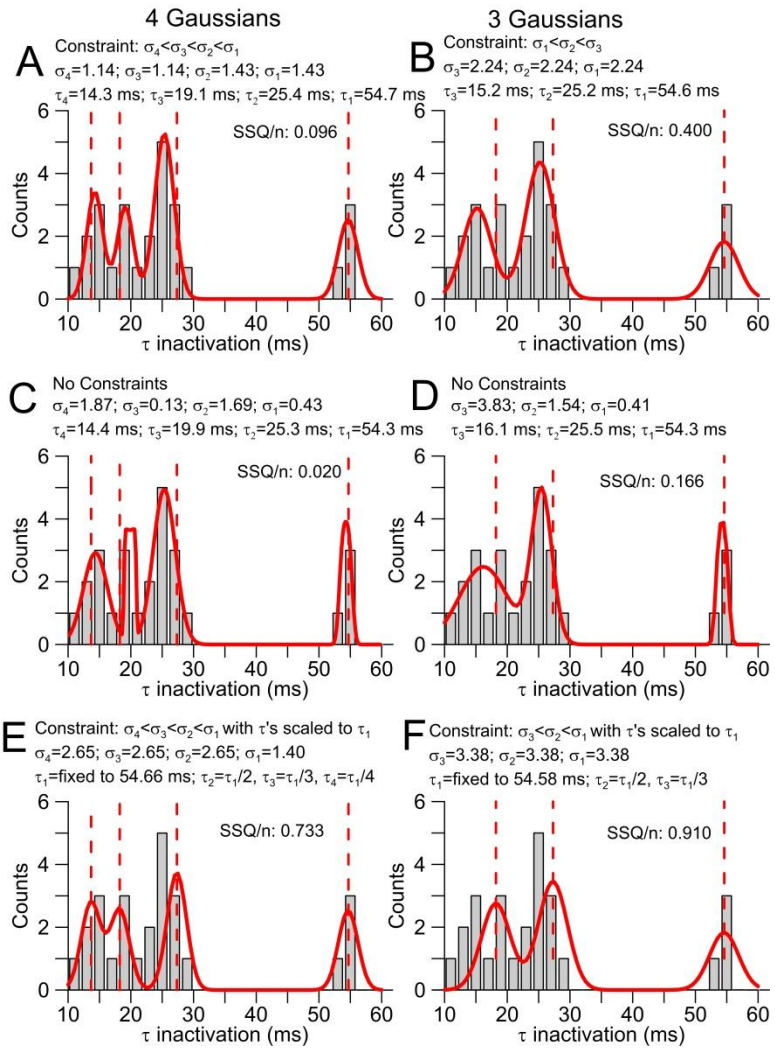

Fig. S6. Comparison of 3 and 4 component Gaussian fits to distribution of β2γ1Chim inactivation time constants. (**A**) Fit shown here corresponds to that in **Fig. 4E**, but highlights details of the fitting constraints, with $\sigma4 \leq \sigma3 \leq \sigma2 \leq \sigma1$, with the resulting standard deviations and time constants as indicated. Dotted lines correspond to expected mean time constants based on value of slowest time constant, showing reasonable correspondence to observed distributions. (**B**) 3 Gaussian fit is as in **Fig. 4F**, but with details shown. To accommodate constraint that $\sigma3 \leq \sigma2 \leq \sigma1$, fitted distributions are excessively broad particularly for faster time constants, and the fitted peaks deviate from the expectation that $\tau_2=0.5*\tau_1$, and $\tau_3=0.33*\tau_1$. (**C, D**) Fits with all parameters unconstrained are shown for 4 (**C**) and 3(**D**) component Gaussians. Although the number of entries are insufficient to describe each component precisely, the 4 Gaussian fit is better than the 3 Gaussian fit at describing the overall distribution, with the 3 component Gaussian requiring a particular broad standard deviation for the briefest component, consistent with the idea that this component arises from two separate peaks. (**E,F**) Panels compare fits obtained with no only standard deviations are constrained, but all time

constants are explicitly required to scale with the slowest time constant (i.e., τ_2, τ_3, and τ_4 are $0.5*\tau_1$, $0.33*\tau_1$, and $0.25*\tau_1$, respectively). These constraints result in poorest quality fits, but the 4 component fit better captures the overall distribution, while the 3 component fit fails to account for the fast inactivating channels seen in the first three bins.

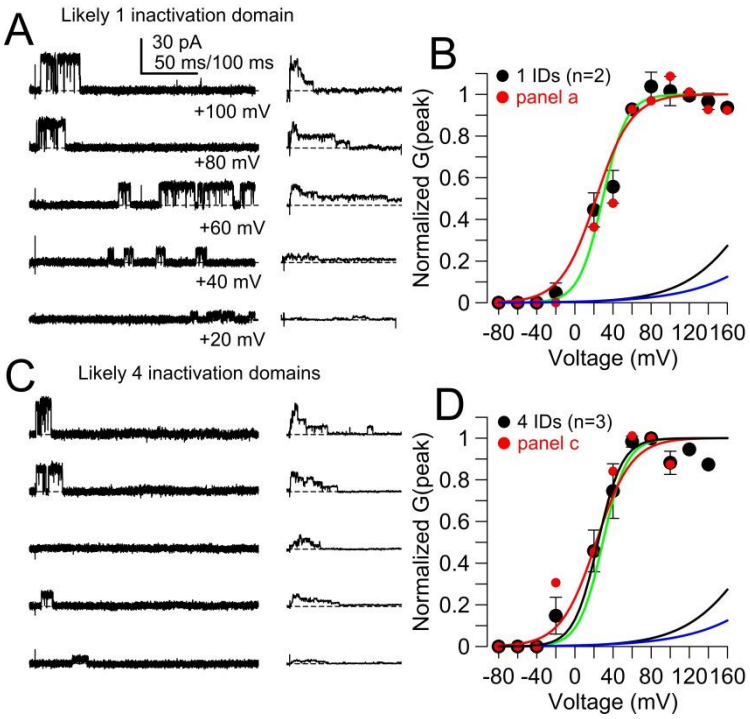

Fig. S7. Channels with one or four β2γ1Chim subunits have similar gating shifts. (**A**) Traces show openings at 0 Ca^{2+} for a single channel in which the averaged τ_i was from the most slowly inactivating group. Openings were readily observed at all voltages above 0 mV. Averages of openings were collected from -80 to +100 mV (right hand traces) and the peak amplitude of the current average was measured. (**B**) The normalized peak conductance for the patch in ***a*** (red circles) is plotted as a function of voltage along with the average of 2 patches (black). Fitted green line (with 90% c.l.) corresponds to V_h=24.8±2.8 mV (z=1.43±0.05e), for the averaged data. Red line is fit to macroscopic GV for α+γ1 channels (**Fig. 3B**; V_h=22.4±2.8 mV). Blue and black lines correspond to GV curves at 0 Ca^{2+} for α+β2 and α alone, from **Fig. 3B**. Additional patches from the slowest inactivating component did not allow full Po/V curves to be generated, but exhibited clear channel activation at +20-+40 mV. (**C**) Traces show openings at 0 Ca^{2+} for a single channel from the most rapidly inactivating β2γ1Chim group with averages of 5 or more sweeps on the right. (**D**) Normalized peak conductance for the patch in c (red symbols) and the average for a set of three patches (black) are plotted as a function of voltage. Fit to averaged data corresponds to V_h=18.3±8.1 mV (z=1.4±0.1e). Green line is the fit to averaged data in panel **B**, with blue and black lines as in **B.**

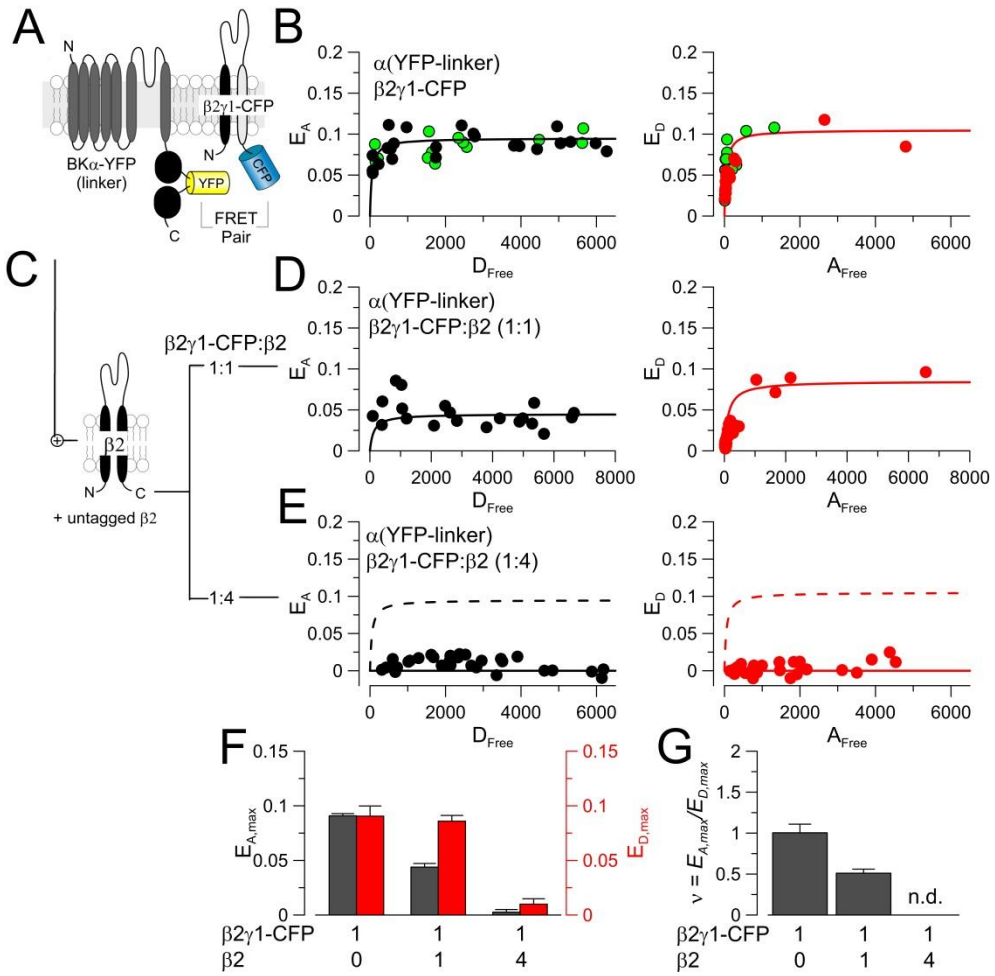

Fig. S8. Coexpression of WT β2 with β2γ1Chim-CFP shows that the average limiting stoichiometry of β2γ1Chim per channel complex is reduced presumably by displacement with β2. (**A**) FRET signals were generated with the BKα-YFP(linker) acceptor and the β2γ1Chim-CFP donor. (**B**) E_A (left) is plotted as a function of D_{Free} and E_D (right) as a function of A_{Free} for cells transfected with BKα-YFP and β2γ1Chim-CFP. Green symbols are from the experiments summarized in Fig. S3C-D. Black and red symbols are from a separate set of transfections, specifically testing the impact of WT β2 competition. (**C**) The WT β2 subunit was coexpressed at two β2γ1-CFP:β2 ratios. (**D**) At a 1:1 β2γ1Chim:β2 ratio, maximal E_A is reduced (left) relative to maximal E_D (right). (**E**) At 1:4 β2γ1Chim:β2, changes in E_A and E_D are essentially undetectable. (**F**) E_A and E_D are plotted for each β2γ1Chim:β2 expression ratio. (G). The average stoichiometry of donors to acceptors in the BK:β2γ1Chim FRET complex determined from $E_{A,max}/E_{D,max}$ is plotted for each expression ratio, showing that increases in WT β2 reduce the average limiting number of chimeric subunits per channel.

References

1. Gonzalez-Perez V, Xia XM, & Lingle CJ (2014) Functional regulation of BK potassium channels by gamma1 auxiliary subunits. *Proc Natl Acad Sci U S A*.
2. Wang Y-W, Ding JP, Xia X-M, & Lingle CJ (2002) Consequences of the stoichiometry of *Slo1* α and auxiliary β subunits on functional properties of BK-type Ca^{2+}-activated K^{+} channels. *Journal of Neuroscience* 22:1550-1561.
3. Erickson MG, Alseikhan BA, Peterson BZ, & Yue DT (2001) Preassociation of calmodulin with voltage-gated Ca(2+) channels revealed by FRET in single living cells. *Neuron* 31(6):973-985.
4. Ben-Johny M, Yue DN, & Yue DT (2016) Detecting stoichiometry of macromolecular complexes in live cells using FRET. *Nat Commun* 7:13709.